IEEE Transactions on Aerospace and Electronic Systems, Available online 15 March 2022
DOI:10.1109/TAES.2022.3159317

An Integrated Approach for On-Demand Dynamic Capacity Management Service in U-space

Yiwen Tang*, Yan Xu† and Gokhan Inalhan‡
Cranfield University, Bedford, MK43 0AL United Kingdom

This paper presents an integrated approach for on-demand Dynamic Capacity Management (DCM) service to be offered in U-space. The approach involves three main threads, including flight planning (demand), airspace configuration (capacity) and demand-capacity balancing (DCB). The flight planning thread produces UAS (unmanned aerial systems) trajectories for each flight that together reflect the estimated traffic demand. The airspace configuration thread defines the fundamental airspace structure and proposes dynamic adjustment schemes that determine the capacity distribution. It also enables the flight planning to reschedule alternative trajectory options to route away from possible congested areas. The last DCB thread takes the previous inputs and then computes for the optimal slot allocation and trajectory selection, as well as the optimal airspace configuration. Simulation case studies have been performed through mimicking an envisioned U-space operating scenario. Results suggest that the integrated approach can achieve the best outcome in almost all the key performance areas than any other cases where only partial functions are realised.

*PhD candidate, Centre for Autonomous and Cyber-Physical Systems, School of Aerospace, Transport and Manufacturing.
†Lecturer in ATM/CNS, Centre for Autonomous and Cyber-Physical Systems, School of Aerospace, Transport and Manufacturing.
‡Professor in Autonomous Systems and Artificial Intelligence, Centre for Autonomous and Cyber-Physical Systems, School of Aerospace, Transport and Manufacturing.

Nomenclature

$f \in \mathcal{F}$	set of *linear* flights
$a \in \mathcal{A}$	set of *area* flights
$k \in \mathcal{K}$	set of trajectory options
$j \in \mathcal{J}$	set of *elementary* cells
$t \in \mathcal{T}$	set of time moments
$\tau \in \mathbb{T}$	set of time periods
$u \in \mathcal{U}$	set of airspaces
$s \in \mathcal{S}$	set of *configurations*
$l \in \mathcal{L}$	set of *operational* cells
$\mathcal{K}_f$	subset of trajectory options for f
$\mathcal{J}_k$	subset of *elementary* cells that k traverses
$\mathcal{J}_a$	subset of *elementary* cells that a traverses
$\mathcal{J}_u$	subset of *elementary* cells defined by u
$\mathcal{T}_k^j$	subset of feasible time moments for k to enter j
$\mathcal{T}_a^j$	subset of feasible time moments for a to enter j
$\mathcal{S}_u$	subset of *configurations* of u
$\mathcal{S}_l$	subset of *configurations* composed of l
$\mathcal{K}_{f,\tau}^{j,j'}$	subset of f's trajectories whose feasible time moments of entering j or j' overlap with τ
$\mathcal{A}_\tau^j$	subset of *area* flights whose feasible time moments of entering or exiting from j overlap with τ
$\mathcal{J}_k^{(i)}$	i^{th} $(1 \ldots n)$ *elementary* cell of k
$\mathcal{J}_a^{(i)}$	i^{th} $(1 \ldots n)$ *elementary* cell of a
$\overline{\mathcal{T}}_k^j$	upper bound of feasible time moments $\mathcal{T}_k^j$
$\underline{\mathcal{T}}_k^j$	lower bound of feasible time moments $\mathcal{T}_k^j$
v_f	weighted costs of priority level for f
v_a	weighted costs of priority level for a
r_k^j	scheduled time of trajectory k to enter j
$\hat{t}_a$	scheduled flight duration of a
$\hat{t}_k^{jj'}$	scheduled flight time between segment jj' of k
$\overline{\mathcal{J}}_k^l$	*elementary* cell by which k exits from l
$\underline{\mathcal{J}}_k^l$	*elementary* cell by which k enters l
$\underline{\mathcal{J}}_a^l$	*elementary* cell by which a enters l
c_u^τ	entry count capacity of u during τ
c_l^τ	occupancy capacity of l during τ
d_f^k	extra flight time flown by k of f
α	unit cost of extra flight time
β	unit cost of delay
γ	unit cost of supplying occupancy capacity
ϵ	superlinear coefficient of delay cost
M	artificial parameter of a large positive value

I. Introduction

It is envisioned that unmanned aerial systems (UAS) will be part of our future in the sky. The growing market shows significant potential across the world, with demand in Europe estimated in excess of EUR 10 billion annually by 2035 and over EUR 15 billion annually by 2050 [1]*. Opening the sky, in particular for (but not limited to) Very Low Level (VLL) airspace, to these new entrants means a move from several thousand conventional aircraft in the sky every day to potentially hundreds of thousands of aerial vehicles, including in urban cities where the density and ground risks are expected to be higher. Thus, a dedicated UAS traffic management (UTM) system is in urgent need to achieve the smooth, safe and fair integration of UAS into the airspace [2].

This includes U-space in Europe, coordinated by SESAR JU (Single European Sky ATM Research Joint Undertaking), which stands for a set of new services and specific procedures designed to support safe, efficient and secure access to airspace for large numbers of drones, relied on a high level of digitalisation and automation of functions [3]. Similar activities exist in the US, led by NASA (National Aeronautics and Space Administration) and partnered with the FAA (Federal Aviation Administration) and industry, aiming at defining an ecosystem for uncontrolled operations that is separate from, but complementary to, the air traffic management (ATM) system [4]. China, another major country in the drone market, leading the production of leisure units, has also launched its pilot UAS traffic management program. A trial Information Service System has been introduced by CAAC (Civil Aviation Administration of China), offering services including flight approval, real-time flight path monitoring, identification and information broadcasting [5]. Parallel activities being conducted in other states, at different stages, can be also noticed (see Australia [6] and Brazil [7] for instance). In this paper, for clarity, we will focus on the case of U-space.

The seamless integration of UTM and ATM is critical to fully unlock the potential benefits of UAS applications. Alongside the integration of UTM with the ATM system, an emerging Urban Air Mobility (UAM) focusing on passenger or cargo-carrying air transportation using specific corridors within an urban environment aims to further expand such integration towards the concept of Advanced Air Mobility (AAM). In 2020, the FAA and Airservices Australia published their first Concept of Operations for UAM [8, 9]. The envisioned integrated system will be capable of managing aircraft operations of all types, using most efficiently the information exchange and the supporting infrastructures, without the need for segregation to separate airspace for manned and unmanned traffic.

As the conventional air transportation demand constantly grows, air traffic flow and capacity management (ATFCM), one of the three pillars of ATM (along with air traffic services and airspace management), has been playing an increasingly important role. Its main objective is to balance the traffic demand and airspace capacity, in such a way that an early-stage safety net can be built to protect the air traffic control (ATC) from being overloaded. Likewise, the fast

*The forecast may be subject to further adjustment due to Covid-19 impact.

growing of UAS demand will eventually approach the airspace threshold, and thus similar ATFCM initiatives may be also required. According to the U-space Roadmap, a service of Dynamic Capacity Management (DCM) is expected to be achieved at U3 stage which could support more complex operations in dense areas and may include capacity management and assistance for conflict detection. While the detailed definition and the applicable environments are subject to ongoing research and development, an indicative description of this service is quoted below:

Upon the definition of drone density thresholds (that can be dynamically modified), the service monitors demand for airspace, and manages access to that airspace as new flight notifications are received. This service may be coupled with the flight planning management service. There should be appropriate set of rules and priorities for slot allocation when a portion of airspace is expected to reach its capacity limits. Apart from the demand and capacity balancing, the service could manage capacity due to non-nominal occurrences, such as weather hazards or emergency situations. [10].

Motivated from the above description, this paper proposes an approach towards the indicated DCM service, in which a set of functions are enabled encompassing flight planning, slot and trajectory allocation, and capacity optimisation. This integrated approach produces an optimal solution minimising the operational costs while maintaining traffic density under the airspace thresholds. It has been simulated under the proposed framework with a scenario of future U-space operations, testing also different cases where some partial functions are disabled.

The anticipated DCM service seems to have a high level of similarity to the conventional ATFCM, in the sense of their rationale and methodology. Recent studies have shown this trend as well. For example, [11] presented a formulation of the UAS traffic flow management problem, which can be traced back to a classical ATFCM model [12]. Based on that formulation, the authors further discussed the trade-off between efficiency and fairness, which was also addressed precisely in the ATFCM domain by [13]. As an early effort to incorporate UAS trajectories into airspace and airport resource sharing schemes, [14] proposed a distributed system that would enable autonomous trajectory planning by manned and unmanned aircraft, while optimising system-wide objectives. Another way of modelling the UAS traffic flow is, rather detailing individual aircraft, to spatially aggregate it on a route/area basis, as studied by [15], aimed at urban scenario with a novel lane-based airspace structure. Previous work in this vein for conventional aircraft can be appreciated from [16, 17] which could be used to capture the traffic flow characteristics in a similar way.

The lessons learned from conventional airspace capacity management can be also useful, for instance sector redesign [18] and dynamic sectorisation [19] or, less ambitious but realistic, flexible opening of predefined airspace configurations [20]. Once the traffic density increases, the airspace will be layered for air traffic control officer (ATCO) [21]. These initiatives aim to keep the manageable workload for ATCO by decomposing the air traffic services. Such principle may also help ensure the tractability of the U-space system when dealing with high-density traffic scenarios. However, in many cases the solutions may not directly apply to U-space, due to their differences in various operational features, even the fundamental airspace structure. In response to this issue, researchers proposed a wide variety of concepts, such as lanes (corridors) and traffic lights [15], roundabout-like intersections [22], road-based two-way and one-way streets on a

horizontal structure [23], and a comparison via large-scale simulations conducted by [24] across four concepts involving full-mix, layers, zones and tubes.

More recently, [25] presented a performance-based airspace model, using a set of elementary cells as the reference grid, associated with the UAS protection volume that depends on its CNS (communication, navigation and surveillance) performance. A close framework can be found in DLR (German Aerospace Centre) Blueprint, introducing its concept for urban airspace integration [26]. This Blueprint describes a U-space management system enabling dynamic airspace configuration and traffic management. It foresees that the airspace will be segmented into a virtual multi-dimensional map, specifically into cells of similar requirements on airspace usage. Each cell might be used by few UAS with a large ellipsoid that relies on flight approval, technical capabilities and performance parameters, thus quickly reaching the cell's capacity, or it could be used by more UAS with a smaller ellipsoid.

The fundamental element of DCM is, besides the structured airspace, the flight plans or more precisely the planned UAS trajectories, which is similar as conventional aircraft trajectories to ATFCM (in particular under the paradigm of Trajectory Based Operations [2]). Depending on the user needs, there are various out-of-the-box tools available in the market, some of which are integrated with the flight control system, for instance [27, 28]. These tools enable a fast and easy access for average users to plan their flight missions, although not officially approved yet as a means for fully automated Beyond Visual Line Of Sight (BVLOS) operations at scale. Generally, they can be considered as the routing or path planning problem, and there have been a wide range of research dedicated to another closely related problem that is trajectory computation and optimisation. A fast chance-constrained trajectory generation strategy incorporating convex optimisation and convex approximation of chance constraints was proposed in [29] to solve the UAS path planning problem. To guarantee the smoothness of flight trajectories, a trigonometric series-based trajectory optimisation approach is developed in [30] to generate smooth flight trajectories. Further more, in response to high-density urban environments, a route network-based flight planning problem for multiple UAS was studied in [31]. A path planner consisting of both global and local planning based on a complete autonomous architecture was presented in [32].

The main contributions of this paper are summarised as follows: (1) an integrated DCM approach is proposed, coupling a demand thread (i.e., flight planning management), a capacity thread (i.e., dynamic airspace configuration), and a joint demand-capacity balancing (DCB) thread as dipicted in Fig. 1; (2) a DCB model is presented, optimising the slot/delay allocation, trajectory selection and airspace configuration as a whole; (3) the metrics of both entry count and occupancy are incorporated into the DCB optimisation model as capacity constraint; and (4) a virtual scenario of U-space operations is set up and simulated to evaluate the effectiveness of the proposed approach.

The rest of this paper are organised as follows: Sec. II introduces the fundamental functions of UAS flight planning. Sec. III envisions the way how VLL airspace might operate, and thus the expected dynamic capacity management. Then, Sec. IV focuses on the DCB optimisation model which is the core of DCM, supported by alternative trajectory

option (ATO) and dynamic airspace configuration (DAC). Numerical experiments are performed in Sec. V through four illustrative examples. Finally, Sec. VI summarises the conclusions and the future work. Additional numerical experiments are presented in Appendix A.

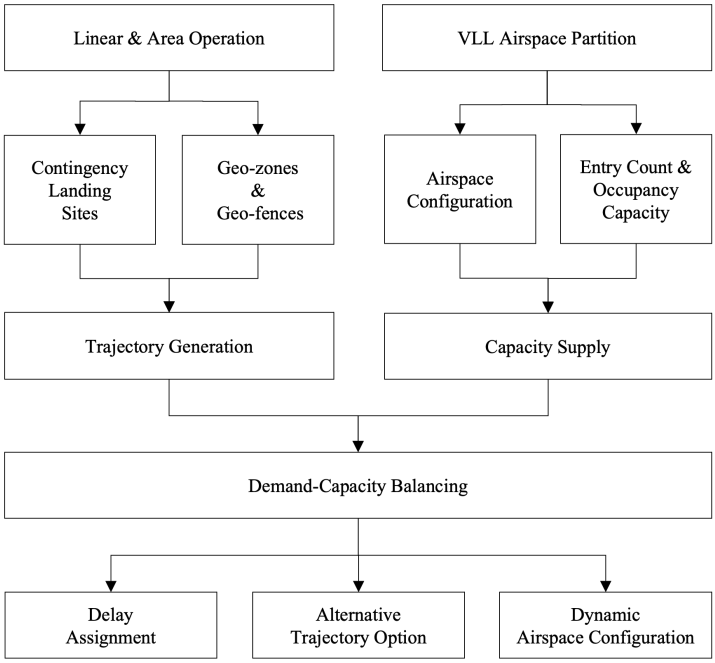

Fig. 1 Workflow of the integrated DCM approach

II. UAS flight planning management

This section introduces a preliminary study for UAS flight planning management, taking into account constraints including the geographical zones, geo-fences and contingency landing sites. This initial study does not compute trajectory of high-fidelity that usually requires a detailed analysis of vehicle dynamics and performances. The trajectories used in this paper are only to reflect the flight intent, specifically the temporal-spatial traffic demand. However, the proposed DCM approach is generic to have both high- and low-fidelity trajectories as input.

A. Types of operation

According to [33], generally there are three main types of UAS operations, namely remotely piloted, automated and formation/swarming flights. Further in terms of the remotely piloted flight, it involves Visual Line Of Sight (VLOS) and Beyond VLOS (BVLOS). We will look into their commonality in representing traffic demand.

Fig. 2 shows a schematic of the commonly-seen UAS trajectories. The planned trajectory might be associated with a "buffer space" because of uncertainties [33]. The yellow stripe around the precise trajectory (green curve) represents

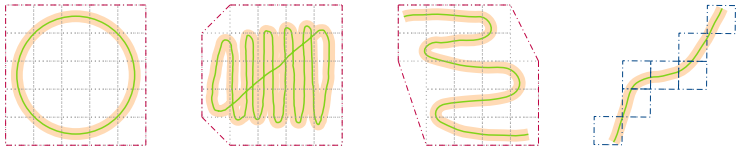

Fig. 2 Schematic of *area* and *linear* UAS trajectories with uncertainty buffers, adapted from [33].

such buffer. We can reshape (using grids) and then group them into two types, namely *area* and *linear* operations, as highlighted in red and blue grids respectively. Depending on the size of the buffer space, the involved grids may vary.

The difference between *area* and *linear* operations can be noticed from the time and space features of those trajectories. Concretely, with the *area* type of operation, certain positions (i.e. grid in this case) may be revisited by the UAS for multiple times, while with the *linear* type, it traverses each position for only one time. Based on such classification, we will discuss these two types of trajectories throughout the paper.

B. Geographical zones and geo-fences

The full integration of airspace used by manned and unmanned aircraft is envisioned in the future as a viable solution to accommodate ATM as a whole [34]. However, as [35] states, the current technologies and the maturity of the U-space services and DAA (Detect and Avoid) systems do not allow for such a level of integration. Therefore, today's airspace management techniques such as segregation and use of restricted and dangerous areas will still play an important role in VLL airspace, as they are necessary for safety.

The EU Implementing Regulation 2019/947 [36] Article 15 enables the creation of geographical zones (geozones) that prohibit or restrict access to drones for safety, security, privacy or environmental reasons. The creation of geozones is based on competencies of authorities at different levels, and each geozone will be tied to an authority responsible for authorising operations. For example, the UK CAA (Civil Aviation Authority) runs a form of "geographical zoning" within the existing manned aviation airspace reservations (Prohibited, Restricted and Danger Areas, along with their "temporary" variants) and the Flight Restriction Zone system that is in place around protected aerodromes [37].

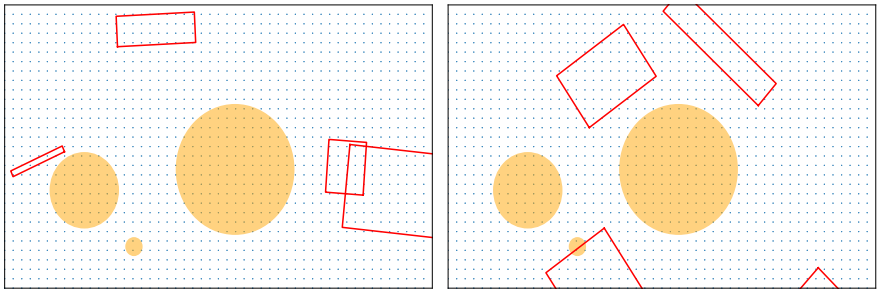

(a) Time 1 (b) Time 2

Fig. 3 Fixed geographical zones (yellow circle) and dynamic geo-fences (red rectangle)

.

In addition to the geozones (see the yellow circles in Fig. 3) that are more of a strategic (long-term) measure, there is another restriction closer to the short-term phase, namely the geo-fences (sometimes referred to as geo-cages) that are defined by the (dynamic) geo-fencing service. They are geographic boundaries which should be respected during the UAS operations. The geo-fences' information will be provided through the geo-awareness service, and will have to be shared with the operators as early as possible (some of which may affect the UAS already in the air). For simplicity, we consider the time-varying geo-fences (see the red rectangles in Fig. 3a and 3b) based on the operation's planned take-off time, meaning that only those defined at the time when a UAS is scheduled to depart will be taken into account.

C. Contingency/emergency landing sites

Today's UAS techniques may involve significant operational uncertainties that could lead to undesirable consequences, e.g., the UAS experiencing a loss of datalink or a failure of flight controller, or on the ground the remote pilot committing a critical human error. As a result, the UAS operation plan may include contingency plans, or emergency response plans, to be followed in case of contingency or emergency. As illustrated by [33], these may include alternate landing sites or more complex procedures.

This paper considers the use of alternate landing sites. The planned trajectory will be subject to a constraint that the UAS must remain in range of an adequate landing site at any time through the operation. This is similar to the regulation for commercial aviation in early days (when aircraft were not extremely reliable). The idea is to allow the UAS in contingency/emergency to land at a dedicated spot within a certain period of time (recall the Extended-range Twin-engine Operational Performance Standards (ETOPS) in manned aviation [38]).

The green circles in Fig. 4 represent areas that are in range of various (arbitrary) landing sites. For convenience, we use a fixed distance to all these sites, although it may be better to specify a time-based rule. Nevertheless, the effects of including such alternate landing sites in trajectory generation can be appreciated from Fig. 4. For the *linear* operation, the blue one (maintaining a range to available landing sites), flies a longer distance than the red one (without considering

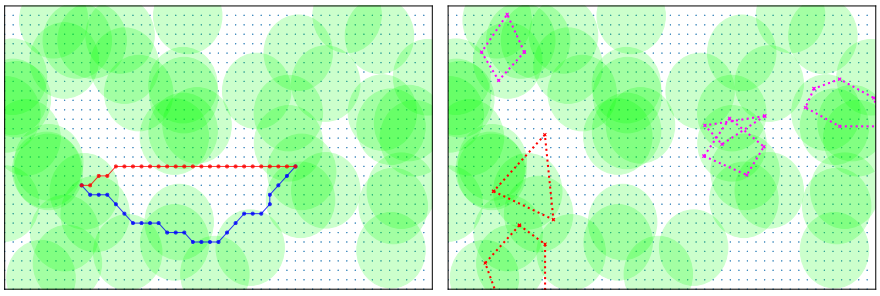

(a) *linear* operation (b) *area* operation

Fig. 4 Operations with and without taking alternate landing sites. (a) red color without site, blue one with; (b) red color without site, purple ones with.

any site). For the *area* operation, the purple ones are fully in the range, while the red ones cannot be approved, as part of their coverage is out of the range to any available landing site.

D. Trajectory generation

Given the above discussion, we then generate the trajectory subject to those constraints. Recall the grid-based trajectories shown in Fig. 2 for *linear* and *area* operations. The airspace is mapped by a set of elementary grids. Each grid is connected to its adjacent in 8 directions (except for those on the boundary), and is represented by a central point, as shown in Fig. 5. Obviously, the more grids we use for a piece of airspace, the more accurately a trajectory can be reflected. We assume a 2D plane in this paper and a further extension to 3D volume is under investigation which indeed increases the problem complexities such as airspace structure modelling and UAS vertical profile planning.

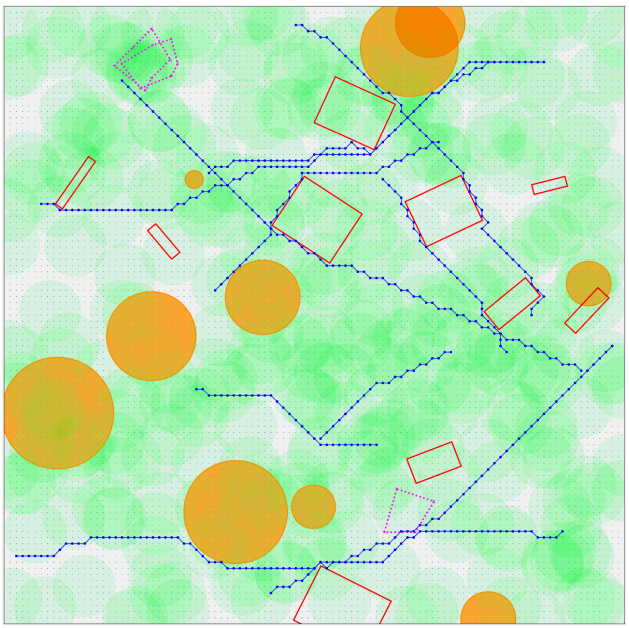

Fig. 5 Generated UAS trajectories in VLL airspace, involving *linear* trajectories (blue curves), *area* trajectories (purple polygons), geozones (yellow circles), geo-fences (red rectangles) and contingency/emergency landing sites (green areas).

To generate the *linear* trajectory, we apply the commonly-used A* algorithm [39], searching for the shortest path composed of a set of sequential grids (see examples with blue curves in Fig. 5). It should be noted that alternative algorithms (e.g., Pure-Pursuit [40]) could be also adopted to avoid non-optimal unrealistic paths with sharp turns. Depending on the buffer space (for uncertainty), additional grids can be included into that sequence. For simplicity, we consider only the original ones (see the blue dots). On top of the fixed path, we then attach the time stamp, starting from a take-off time at its first point, and iterating over each segment given an assumed speed, until reaching the last point for landing time.

With regard to the *area* trajectory, we consider a (random) set of vertices to define the boundary of an operation.

Each edge is similar to the segment of *linear* trajectory, which in turn is subject to all the constraints mentioned above (fixed geographical zones, dynamic geo-fences and contingency/emergency landing sites). The major difference, however, lies in their time stamps. Considering that some grids might be revisited several times for an *area* trajectory (recall Sec. II.A), we simply fix the same period of operational time for all the traversed grids, rather than specifying a unique time stamp for each grid (as done for the *linear* trajectory). In short, there are only two times associated with an *area* trajectory, namely the take-off and landing times that remain the same across all the concerned grids.

III. Dynamic capacity management

As foreseen in Swiss U-Space[†], when users are competing for airspace, the DCM service will provide negotiation capabilities and operation planning tools (e.g., route planning functions, airspace configuration options) to support collaborative decision making and/or offer alternatives. This will allow equitable access to airspace and optimise its use by resolving demand-capacity imbalances [41]. In this section, we discuss a primary partition of the VLL airspace into *elementary* cells. Based on that partition, two supporting tools are presented to enable alternative trajectory option (ATO) and dynamic airspace configuration (DAC).

A. VLL airspace partition

In conventional manned aviation, when traffic demand is expected to be higher than airspace capacity, the provision of air traffic services will be decomposed in the different sectors [21], into tasks with manageable workload for human controllers and facilities [‡]. As such, with UAS traffic levels (density especially), tractability of the system under a single cell becomes hard, also from a human factors point of view. In U-space, while the airspace definition and capacity management are still at a very early stage, it is widely recognised that the "full" of an airspace will be related to the probability of flights to lose safe separation [33]. According to the Air-Risk Class proposed by [43], one of the ways to reduce collision risk is to control the geometry of the flights within an airspace. An intuitive example would be cars on the two-way road system. By controlling the geometry of flights through airspace structures, procedures, and regulations, collision risk can be greatly reduced.

Following this thought, it is possible that such geometry parameter may eventually lead to VLL airspace partition (similar as done in ATM). Imagine a group of roads/corridors, along with the restriction/geographical zones, geo-fences, urban infrastructures and communication coverage areas, just to name a few, share the same piece of airspace, probably interacting with each other. A broader rule of airspace classification (such as type X, Y and Z Volumes in U-space) can pose general procedures and regulations across that airspace, whilst a further definition of its substructures may result to better decomposition of the U-space service provisions, leading to increased scalability of the U-space implementation.

[†]The first nationwide U-space system in Europe.

[‡]A sectorless operation concept has been recently demonstrated in [42], in which the workload is distributed among controllers instead of sectors. One key rationale is the lack of available controllers towards the growing traffic demand. This may differ than the case in U-space, where a common understanding is that higher levels of automation are expected, lowering down human involvement where appropriate.

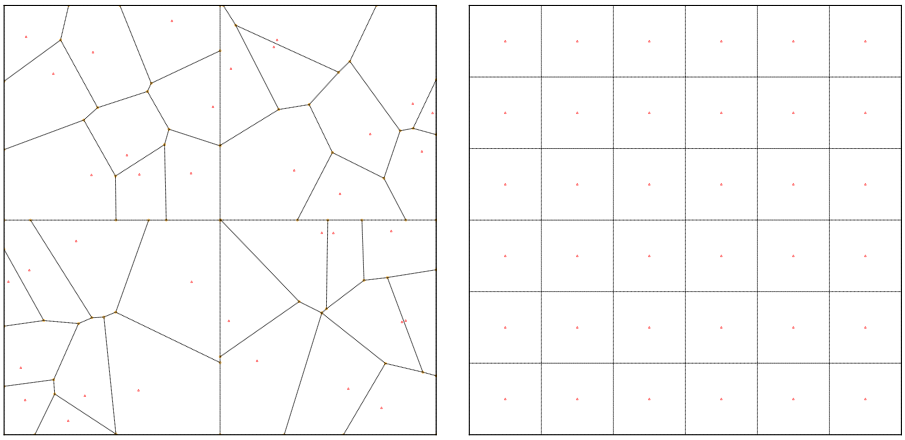

(a) Voronoi-based partition (b) Grid-based partition

Fig. 6 VLL airspace partitioned into static *elementary* cells.

To this end, we apply a primary partition to the VLL airspace. The Voronoi Diagram described in [44] is used to divide the airspace into a set of static *elementary* cells. Using this algorithm, a 2D space can be partitioned into convex polygons such that each polygon contains exactly one generating point and every point in a given polygon is closer to its generating point than to any other. As a consequence, the original partitioning problem can be converted to finding the optimal generating points. This new problem is out of the scope of this paper and deserves a separate careful discussion. As shown in Fig. 6, we sample from a random distribution to those points, and run the Voronoi algorithm to generate all the *elementary* cells (see Fig. 6a). Note that another oversimplified case would be grid-like partitions (see Fig. 6b).

B. Alternative trajectory option

On top of the fixed *elementary* cells, we then include the previously generated flight trajectories. The interactions between trajectory and airspace can be easily derived. As shown in Fig. 7, the yellow curve represents an initially planned *linear* trajectory, and the *elementary* cells that this flight is scheduled to traverse are highlighted.

Assuming any portion of the airspace becomes full, therefore turning into a hotspot, the flight can either hold on at some point (or change speed) to shift the timing when it will arrive, or it can route away from the full airspace. In the latter case, we can generate the rerouting trajectory using the same method when planning the initial trajectory, incorporating additional geographical constraints. Fig. 7 presents all the feasible alternative options (see blue curves) that bypass each of the associated *elementary* cells (except for the first and last ones for take-off and landing). This is realised by applying the same A* algorithm for path finding here, whereas the connectivity of some specific grids is further turned off. Those grids are around the boundary of an *elementary* cell, and turning them off will prohibit a path entering into it. Also, they are updated for each associated *elementary* cell in such a way that only one cell is avoid for one rerouting trajectory option.

In addition to the above hotspot-avoidance trajectories, alternatives for any other reason are also applicable, for instance if there is a temporal close of airspace. In any case, extra flight distance (time) might be incurred by taking the alternative options. Note that rerouting (i.e., alternative trajectory option) is not applicable to the *area* operations, meaning that these flights will be subject to only delay regulations.

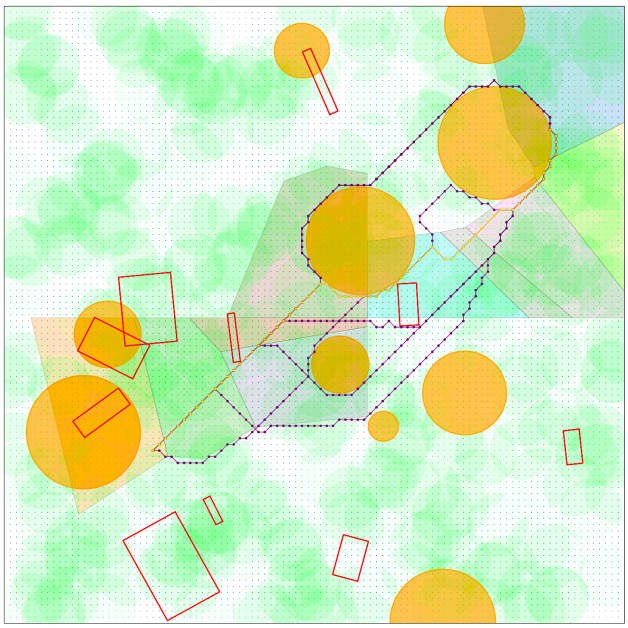

Fig. 7 *Linear* operation's alternative trajectory options to route away from each associated *elementary* cell (transparent polygons), where yellow curve represents the initially planned trajectory and purple curves are the hotspot-avoidance alternatives.

C. Dynamic airspace configuration

Dynamic capacity management aims to match demand with capacity, namely demand may be regulated to match capacity, or capacity may be changed to match demand. In this section, we consider flexibly adjusting *elementary* cells that focuses on the capacity thread. The effects can be two folded: it enables flexible on-demand capacity provision (e.g., capacity redistributed in line with demand regulation); and it also adjusts the airspace structure to better accommodate the (regulated) traffic flow.

First we clarify some airspace relevant concepts used in this paper. The static *elementary* cells resulted from the partition are the basic unit of airspace, which can act individually as one *operational* cell, or can be merged with its adjacent *elementary* cell(s) to act together as another *operational* cell. A combinatorial status for every *elementary* cell of an airspace is referred to as an airspace *configuration* which could be pre-defined.

Fig. 8 shows an example of 4 *configurations* with respect to 4 airspaces. Obviously, there could be a long list of selectable *configurations* if there exist a large number of *elementary* cells. To make it more realistic, we allow that any adjacent (i.e. with one shared edge) *elementary* cells can be merged, but the maximum number of them within any

single *operational* cell is limited. As such, the time-space distribution of trajectory can be implicitly checked in the next DCB model in terms of the cell occupancy-capacity constraint. Specifically, when an *elementary* cell is extended to an *operational* cell that contains multiple *elementary* cells, each concerned trajectory associated with them will be checked such that their overall occupancy metric is enforced to stay below some threshold. The detailed conflict management for those trajectories (e.g., to avoid cluttered area) will be mainly tackled by another service named Strategic Conflict Resolution (SCR) in U-space which has been reported in [22][45][46]. In this paper, we focus on DCB instead, as SCR in U-space cannot ensure a balanced traffic demand and airspace capacity, while our focus solves this critical problem via an integrated DCM approach.

The capacity of an *operational* cell may depend on various factors, such as the physical shape, weather condition, DAA service and the maturity of supporting techniques, as well as the UAS capability and performance, which is why the capacity should be dynamically modified. According to the recent key findings from [47], capacity is a function of risk-based (including third-party ground and air risk) and social indicators per pre-defined airspace volume. Thresholds are defined for each of these indicators which, in conjunction, define the overall capacity limit of an area. However, the capacity assessment/prediction is beyond the scope of this paper. For convenience, we assume it is only associated with the size of the area, with a discount factor based on the number of merged *elementary* cells (see details in experimental setup). In terms of capacity counting, we consider the metrics of entry count and occupancy.

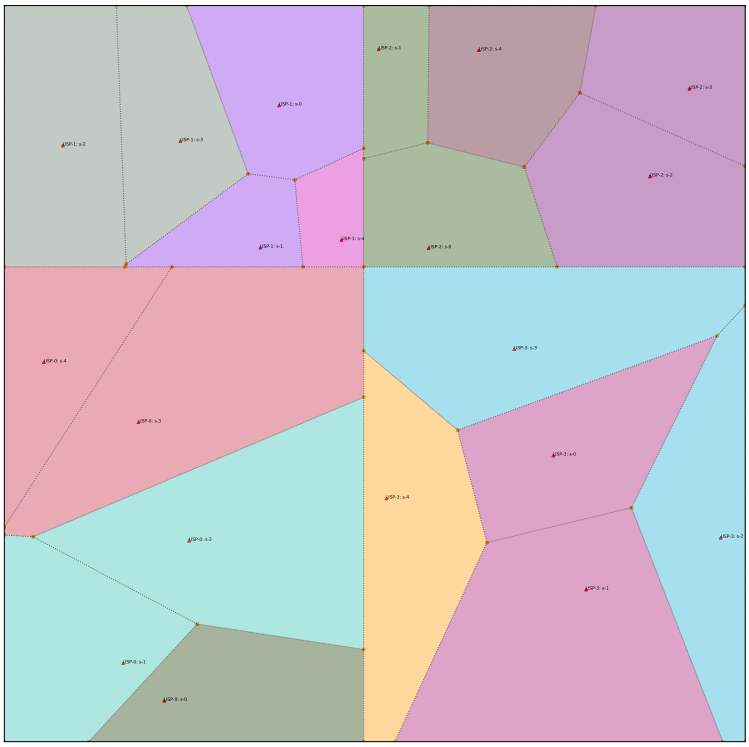

Fig. 8 Example of 4 airspaces' *configurations*, where the same colour represents one *operational* cell that is composed of one or more *elementary* cells.

Finally, we might be still at a stage far from quantifying the monetary cost of running a specific airspace *configuration*, but the implications of capacity may give us some hints. As higher levels of automation are envisioned in UTM, such cost may not come from human controllers (as in manned aviation), but from other aspects that would impose boundaries of the capacity, such as the risks and social impact associated with that airspace volume. In this paper, we consider a linear correlation between the cost of running a *configuration* and the total capacity it can provide.

IV. Demand-capacity balancing model

Given the model input introduced previously in both the demand and capacity threads, along with some explicit and implicit assumptions, this section will present the mathematical formulation of the DCB model. It leverages not only conventional slot/delay assignment, but also the alternative trajectory option (ATO) and dynamic airspace configuration (DAC).

A. Decision variables

The model is formulated by mixed integer linear programming and the corresponding decision variables are defined below:

$$x_{f,t}^{k,j} = \begin{cases} 1, & \text{if } \textit{linear} \text{ flight } f\text{'s trajectory } k \text{ enters } \textit{elementary} \text{ cell } j \text{ by time } t \\ 0, & \text{otherwise} \end{cases}$$

$$z_f^k = \begin{cases} 1, & \text{if } \textit{linear} \text{ flight } f\text{'s trajectory } k \text{ is selected} \\ 0, & \text{otherwise} \end{cases}$$

$$y_{a,t}^{en,j} = \begin{cases} 1, & \text{if } \textit{area} \text{ flight } a \text{ enters } \textit{elementary} \text{ cell } j \text{ by time } t \\ 0, & \text{otherwise} \end{cases}$$

$$u_s^\tau = \begin{cases} 1, & \text{if } \textit{configuration } s \text{ is activated in time period } \tau \\ 0, & \text{otherwise} \end{cases}$$

Note that if the entrance time for an *area* flight has been determined, the exit time will be known as the flight duration is fixed. Also, once a *configuration* is settled, the status of its associated *operational* cells will be also known. Thus, the following two sets of auxiliary variables are considered:

$$y_{a,t}^{ex,j} = \begin{cases} 1, & \text{if } \textit{area} \text{ flight } a \text{ exits from } \textit{elementary} \text{ cell } j \text{ by time } t \\ 0, & \text{otherwise} \end{cases}$$

$$w_l^\tau = \begin{cases} 1, & \text{if } \textit{operational} \text{ cell } l \text{ is opening in time period } \tau \\ 0, & \text{otherwise} \end{cases}$$

Specifically, $w_l^\tau = \sum_{s \in S_l} u_s^\tau,\ \forall l \in \mathcal{L}, \forall \tau \in \mathbb{T}$, where S_l is a subset of *configurations* that are composed (partially) of *operational* cell l. In other words, if any *configuration* related with cell l is selected, then this cell must be open; on the contrary, if the cell will not open (i.e. $w_l^\tau = 0$), then all its concerned *configurations* (S_l) cannot be selected.

An important remark and assumption of this model is that, the time period τ to switch among different *configurations* for each airspace, and the rolling time window τ for capturing demand-capacity situations, are synchronised.

B. Objective function

We consider an objective function composed of two parts with respect to demand and capacity respectively, namely the costs of regulating *linear* and *area* flights, and the costs of supplying airspace capacities. In terms of regulating *linear* flights, the costs can be further divided to delay assignment and flight rerouting.

The delay costs for *linear* and *area* flights can be computed by Eqs. 1 and 2 respectively:

$$C_d^l = \sum_{f \in \mathcal{F}} \sum_{k \in \mathcal{K}_f} \sum_{t \in \mathcal{T}_k^{\mathcal{J}_k^{(1)}}} v_f (t - r_k^{\mathcal{J}_k^{(1)}})^{(1+\epsilon)} (x_{f,t}^{k,\mathcal{J}_k^{(1)}} - x_{f,t-1}^{k,\mathcal{J}_k^{(1)}}), \tag{1}$$

$$C_d^a = \sum_{a \in \mathcal{A}} \sum_{t \in \mathcal{T}_a^{\mathcal{J}_a^{(1)}}} v_a (t - r_a^{\mathcal{J}_a^{(1)}})^{(1+\epsilon)} (y_{a,t}^{en,\mathcal{J}_a^{(1)}} - y_{a,t-1}^{en,\mathcal{J}_a^{(1)}}), \tag{2}$$

where $\mathcal{K}_f$ represents a subset of trajectories selectable by *linear* flight f. $\mathcal{T}_k^j, \mathcal{T}_a^j$ are manually defined subsets of time moments feasible for delay assignment (to reduce model dimension), in which j is at position $\mathcal{J}_k^{(1)}, \mathcal{J}_a^{(1)}$ respectively, meaning the first point (based on *elementary* cell) that the trajectory is scheduled to fly over. The initially scheduled times at that positions are presented by $r_k^{\mathcal{J}_k^{(1)}}, r_a^{\mathcal{J}_a^{(1)}}$ respectively. The superlinear coefficient $\epsilon > 0$ for delay costing is used to evenly distribute the delay across different flights. Also, the flight priority is expressed through a coefficient v_f, v_a to a specific *linear* and *area* flight.

Next, the costs of rerouting can be denoted by Eq. 3, which is only applicable for the *linear* flights.

$$C_r = \sum_{f \in \mathcal{F}} \sum_{k \in \mathcal{K}_f} v_f d_f^k z_f^k, \tag{3}$$

where d_f^k is the additional flight duration of trajectory k compared with the initially scheduled duration of *linear* flight f.

On the airspace side, the associated service cost is reflected by means of the total amount of capacity provision, namely Eq. 4:

$$C_p = \sum_{l \in \mathcal{L}} \sum_{\tau \in \mathbb{T}} c_l^\tau w_l^\tau, \tag{4}$$

where c_l^τ denotes the occupancy capacity supplied through *operational* cell l during the period of time τ.

Finally, the three types of costs are combined as a whole, with weighting cost α set for rerouting, β for delay, and γ for capacity. The equations can be reorganised as follows:

$$\min \quad \alpha C_r + \beta(C_d^l + C_d^a) + \gamma C_p, \tag{5}$$

The constraints are listed below, which can be grouped into individual flight operations, airspace configurations, and traffic entry count/occupancy capacity, as well as the binary condition and space of the decision variables.

C. Individual flight operations

Below constraints are associated with the operational limits with regard to each individual *linear* or *area* flight.

$$\text{s.t.} \quad \sum_{k \in \mathcal{K}_f} z_f^k = 1 \quad \forall f \in \mathcal{F}, \tag{6}$$

$$x_{f,\underline{\mathcal{T}}_k^j - 1}^{k,j} = 0, \; x_{f,\overline{\mathcal{T}}_k^j}^{k,j} = z_f^k \quad \forall f \in \mathcal{F}, \forall k \in \mathcal{K}_f, \forall j \in \mathcal{J}_k, \tag{7}$$

$$y_{a,\underline{\mathcal{T}}_a^j - 1}^{en,j} = y_{a,\underline{\mathcal{T}}_a^j + \hat{t}_a - 1}^{ex,j} = 0, \; y_{a,\overline{\mathcal{T}}_a^j}^{en,j} = y_{a,\overline{\mathcal{T}}_a^j + \hat{t}_a}^{ex,j} = 1 \quad \forall a \in \mathcal{A}, \forall j \in \mathcal{J}_a, \tag{8}$$

$$x_{f,t}^{k,j} - x_{f,t-1}^{k,j} \geq 0 \quad \forall f \in \mathcal{F}, \forall k \in \mathcal{K}_f, \forall j \in \mathcal{J}_k, \forall t \in \mathcal{T}_k^j, \tag{9}$$

$$y_{a,t}^{en,j} - y_{a,t-1}^{en,j} \geq 0, \; y_{a,t+\hat{t}_a}^{ex,j} - y_{a,t+\hat{t}_a - 1}^{ex,j} \geq 0 \quad \forall a \in \mathcal{A}, \forall j \in \mathcal{J}_a, \forall t \in \mathcal{T}_a^j, \tag{10}$$

$$x^{k,j'}_{f,t+\hat{t}^{jj'}_k} - x^{k,j}_{f,t} = 0 \quad \forall f \in \mathcal{F}, \forall k \in \mathcal{K}_f, \forall t \in \mathcal{T}^j_k, j = \mathcal{J}^{(i)}_k, j' = \mathcal{J}^{(i+1)}_k : \forall i \in [1, n), \tag{11}$$

$$y^{en,j'}_{a,t} - y^{en,j}_{a,t} = 0 \quad \forall a \in \mathcal{A}, \forall t \in \mathcal{T}^j_a, j = \mathcal{J}^{(i)}_a, j' = \mathcal{J}^{(i+1)}_a : \forall i \in [1, n), \tag{12}$$

$$y^{ex,j}_{a,t+\hat{t}_a} - y^{en,j}_{a,t} = 0 \quad \forall a \in \mathcal{A}, \forall j \in \mathcal{J}_a, \forall t \in \mathcal{T}^j_a, \tag{13}$$

Constraint 6 states that only one trajectory, among all options, can be selected for each *linear* flight. This constraint is then linked with Constraint 7, where $\mathcal{T}^j_k$ is a subset of feasible time moments for *linear* trajectory k to enter *elementary* cell j, and its upper and lower bound are $\underline{\mathcal{T}}^j_k$ and $\overline{\mathcal{T}}^j_k$ respectively. They specify that, if a trajectory is selected (i.e. $z^k_f = 1$) then it must be assigned with a slot from the set of $\mathcal{T}^j_k$, otherwise (i.e. $z^k_f = 0$) no slot will be assigned. There is no alternative trajectory option for *area* flight, so Constraint 8 enforces that a slot will be assigned at each point. Specifically, as the flight duration $\hat{t}_a$ is fixed, the lower and upper bound of feasible time moments at the "exit" point can be expressed by $\underline{\mathcal{T}}^j_a + \hat{t}_a$ and $\overline{\mathcal{T}}^j_a + \hat{t}_a$, where $[\underline{\mathcal{T}}^j_a, \overline{\mathcal{T}}^j_a]$ are the feasible time moments defined at the "entrance" point.

Next, Constraints 9 and 10 both enforce the continuity of the timeline (recall the concept of *by* time). Constraint 11 stipulates that the controlled flight time between any segment (j, j') of a *linear* flight, remain unchanged than initially scheduled. In the meantime, Constraint 12, with respect to the *area* flight, enforces the controlled times to be the same at all cells covered by that flight. Constraint 13 shows that the duration of any *area* flight does not change from the initially planned.

D. Airspace configurations

The two constraints cover the opening of *operational* cells across the airspace, which is realised by means of selecting (and thus scheduling) a number of pre-defined *configurations*:

$$\sum_{s \in \mathcal{S}_u} u^\tau_s = 1 \quad \forall u \in \mathcal{U}, \forall \tau \in \mathbb{T}, \tag{14}$$

$$\sum_{s \in S_l} u^\tau_s = w^\tau_l \quad \forall l \in \mathcal{L}, \forall \tau \in \mathbb{T}, \tag{15}$$

Constraint 14 states that only one single *configuration* can be selected during each period of time, where $\mathcal{S}_u$ represents the set of selectable options of *configurations* defined beforehand for airspace u. Constraint 15 links the selection of *configuration* and the opening of *operational* cell, as explained previously in Sec. IV.A with regard to the auxiliary variables.

E. Airspace entry count capacity

As a mature and widely-recognised definition of VLL airspace capacity has not reached yet, in this paper we consider to reuse two well-studied metrics in ATM, including entry count and occupancy. Their comparison has been clarified in [48]. Concretely, the entry count is adopted as the measure of airspace's capacity, specifying how many UAS are allowed to enter into an airspace within a certain period of time. The occupancy is meanwhile used as the measure of the *operational* cell's capacity, specifying how many UAS are allowed to appear in a smaller cell's coverage within a certain period of time.

$$\sum_{f\in\mathcal{F}}\sum_{k\in\mathcal{K}_f}\sum_{t\in\tau\cap\mathcal{T}_k^{\mathcal{J}_u}}(x_{f,t}^{k,\mathcal{J}_u}-x_{f,t-1}^{k,\mathcal{J}_u})+\sum_{a\in\mathcal{A}}\sum_{t\in\tau\cap\mathcal{T}_a^{\mathcal{J}_u}}(y_{a,t}^{en,\mathcal{J}_u}-y_{a,t-1}^{en,\mathcal{J}_u})\leq c_u^{\tau}\quad\forall u\in\mathcal{U},\forall\tau\in\mathbb{T}, \tag{16}$$

Constraint 16 states that the number of UAS entries into each airspace must be lower than its capacity in any times. Note that this involves both *linear* and *area* flights, and the coverage and shape will remain unchanged. One major concern of this metric is that the exit time, upon UAS entering a piece of airspace, will not be taken into account. However, the duration of internal movement may still pose workload on the U-space service provision.

F. Cell occupancy capacity

For the occupancy metric, an intuitive example is shown in Fig. 9 and we can see that four cases, including Case-2, -3, -4 and -5, can be regarded as occupancy with respect to period τ_2. As a comparison, only Case-3 and -4 are treated as entry count in the same period. To formalise the calculation, we stipulate that one occupancy will be added, only if the AND condition is satisfied: the flight's entry time is earlier than (or equal to) the period's ending moment, and also the flight's exit time is later than (or equal to) the period's starting moment. To have a clear view, refer to the red and blue lines in Fig. 9.

The main barrier of performing that calculation lies in the judgement of the relationship between a controlled (entrance/exit) time and a period (starting/ending) boundary. Concretely, the feasible time moments $(\mathcal{T}_k^j, \mathcal{T}_a^j)$ will be limited (if compared with the whole time horizon) so as to reduce the dimension of the model. As shown in Fig. 10, the feasible time moments are represented by a stripe of 0/1 numbers, in which a single controlled time will be determined. As this stripe only covers part of the timeline, it is not clear of the situation across all the period boundaries.

For instance, in Fig. 10, the starting of τ_2 (i.e. $\underline{\tau}$) has been highlighted, and only in Case-1 and Case-3 we know exactly if the controlled time is earlier or later than $\underline{\tau}$. In this example, such information of Case-3 is not even useful, because $\underline{\tau}$ should be compared with the flight's exit time, rather than its entrance time.

Therefore, we need a group of helper variables to conduct that judgement. Specifically, $m^{k,j'}_{f,\tau}, n^{k,j}_{f,\tau}$ are defined for the *linear* flights, while $p^{j}_{a,\tau}, q^{j}_{a,\tau}$ for the *area* flights. $n^{k,j}_{f,\tau}, q^{j}_{a,\tau}$ represent if the controlled time of flight (k or a) entering cell j is earlier than (or equal to) the ending moment $\overline{\tau}$ of period τ. On the contrary, $m^{k,j'}_{f,\tau}, p^{j}_{a,\tau}$ denote if the controlled time of flight (k or a) leaving from cell j [§] is later than (or equal to) the starting moment $\underline{\tau}$ of period τ. They can be computed respectively via Eq. 17:

$$\begin{cases} m^{k,j'}_{f,\tau} &= \sum\limits_{t\in[\underline{\tau},\overline{\mathcal{T}}^{j'}_{k}]\cap\mathcal{T}^{j'}_{k}} (x^{k,j'}_{f,t} - x^{k,j'}_{f,t-1}) \\ n^{k,j}_{f,\tau} &= \sum\limits_{t\in[\underline{\mathcal{T}}^{j}_{k},\overline{\tau}]\cap\mathcal{T}^{j}_{k}} (x^{k,j}_{f,t} - x^{k,j}_{f,t-1}) \\ p^{j}_{a,\tau} &= \sum\limits_{t\in[\underline{\tau},\overline{\mathcal{T}}^{j}_{a}]\cap\mathcal{T}^{j}_{a}} (y^{ex,j}_{a,t+\hat{\imath}_a} - y^{ex,j}_{a,t+\hat{\imath}_a-1}) \\ q^{j}_{a,\tau} &= \sum\limits_{t\in[\underline{\mathcal{T}}^{j}_{a},\overline{\tau}]\cap\mathcal{T}^{j}_{a}} (y^{en,j}_{a,t} - y^{en,j}_{a,t-1}) \end{cases} \tag{17}$$

The main idea is to capture the relationship between two boundaries: the bounds of feasible time moments ($\mathcal{T}^{j}_{k}$ or $\mathcal{T}^{j}_{a}$) and the period's boundaries ($\underline{\tau}$ and $\overline{\tau}$). Fig. 10 presents various illustrative cases. Assuming τ_2 is the target period, through Case-1 to Case-6, the shaded 0/1 numbers of every strip in every case are those captured to be added up. Case-0

[§]Cell j' in *linear* flight f represents the next consecutive cell j to be flown by trajectory k, and thus entering cell j' means leaving from cell j.

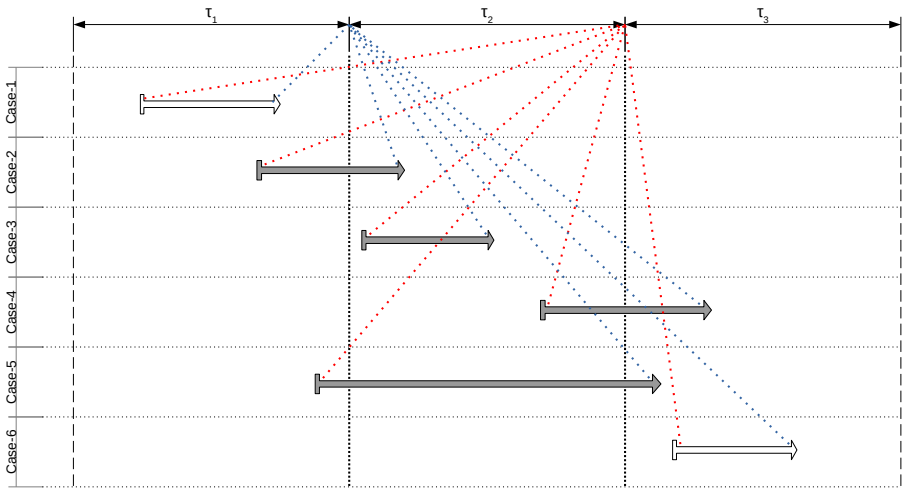

Fig. 9 Measuring occupancy, where the horizontal axis represents the timeline, which is divided into three periods of time (τ_1, τ_2, τ_3). In each case, the starting (square) point denotes the entrance time into a cell, while the ending (arrow) point is the exit time. The red line compares the entry time and the period's ending moment, with the blue line comparing the exit time and the period's starting moment.

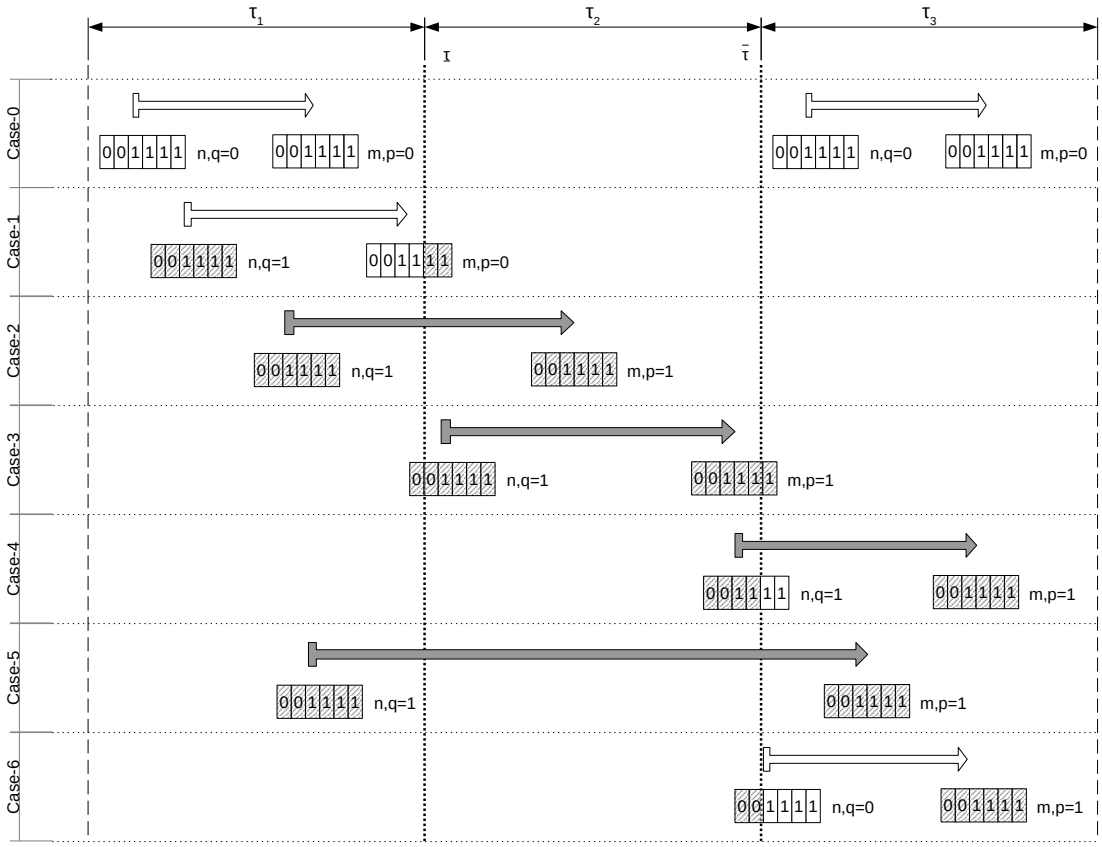

Fig. 10 Incorporating the occupancy metric into DCB modelling architecture.

is an exemption case which we will explain later. The summed values for $n^{k,j}_{f,\tau}$, $q^{j}_{a,\tau}$ and $m^{k,j'}_{f,\tau}$, $n^{k,j}_{f,\tau}$ can be also seen in the figure.

Using the above helper variables, we can then compute the occupancy with the left-hand part of Constraint 18:

$$\sum_{f\in\mathcal{F}}\sum_{k\in\mathcal{K}^{j,j'}_{f,\tau}:j=\underline{\mathcal{J}}^{l}_{k},j'=\overline{\mathcal{J}}^{l}_{k}}(m^{k,j'}_{f,\tau}+n^{k,j}_{f,\tau}-z^{k}_{f})+\sum_{a\in\mathcal{A}^{j}_{\tau}:j=\underline{\mathcal{J}}^{l}_{a}}(p^{j}_{a,\tau}+q^{j}_{a,\tau}-1)\leq c^{\tau}_{l}w^{\tau}_{l}+(1-w^{\tau}_{l})M\quad\forall l\in\mathcal{L},\forall\tau\in\mathbb{T}, \tag{18}$$

where an additional scalar of -1 needs to be further included (recall the AND condition, where only 1 occupancy will be added provided both conditions are met). For the *linear* flights, however, a trajectory k can be either selected, so that this -1 should be associated to z^{k}_{f}.

With regard to the subsets $k\in\mathcal{K}^{j,j'}_{f,\tau}, a\in\mathcal{A}^{j}_{\tau}$ in Constraint 18, it explains why Case-0 in Fig. 10 is an exemption. The period of counting occupancy will roll over the whole time horizon, but it is not necessary to, at each period, look through all flights (or trajectories). The two subsets are therefore used to exclude flights (or trajectories) that are never going to appear in the target period. This will help significantly reduce the model's dimension.

As for the right-hand part of Constraint 18, unlike the fixed coverage considered for each airspace (recall Constraint

16), the actual capacity provision of an *operational* cell l depends on if it is actually opened during period τ. If so, $w_l^\tau = 1$, then the declared capacity c_l^τ has to be respected; otherwise $w_l^\tau = 0$, this Constraint will be relaxed (as M is a large positive number that always makes it feasible).

Worth noting that, while the occupancy metric has been widely adopted in post-regulation DCB performance assessment, it is the first time, to the best of our knowledge, that this metric is used as a pre-regulation constraint in a DCB optimisation model. Further added to the value, it is considered in a context of dynamic airspace configuration.

G. Decision variables conditions

$$x_{f,t}^{k,j} \in \{0,1\} \quad \forall f \in \mathcal{F}, \forall k \in \mathcal{K}_f, \forall j \in \mathcal{J}_k, \forall t \in \mathcal{T}_k^j, \tag{19}$$

$$z_f^k \in \{0,1\} \quad \forall f \in \mathcal{F}, \forall k \in \mathcal{K}_f, \tag{20}$$

$$y_{a,t}^{en,j}, y_{a,t+\hat{t}_a}^{ex,j} \in \{0,1\} \quad \forall f \in \mathcal{F}, \forall j \in \mathcal{J}_a, \forall t \in \mathcal{T}_a^j, \tag{21}$$

$$u_s^\tau \in \{0,1\} \quad \forall s \in \mathcal{S}, \forall \tau \in \mathbb{T}, \tag{22}$$

$$w_l^\tau \in \{0,1\} \quad \forall l \in \mathcal{L}, \forall \tau \in \mathbb{T}. \tag{23}$$

Finally, Constraints 19 - 23 state the binary constraints and domains of the primary and auxiliary decision variables used in the model.

V. Illustrative examples

This section presents the numerical experiments, where we build up an illustrative U-space scenario. The airspace covers a 2D space of $20 * 20\ km^2$, divided by $100 * 100$ grids (being each grid of $0.2 * 0.2\ km^2$). Four case studies have been considered, switching on/off certain DCB initiatives, including delay assignment, ATO and DAC. Results are compared across these cases to demonstrate their impacts on demand-capacity balancing and associated operating costs.

A. Experimental setup

As shown in Fig. 11, the traffic sample includes 296 flights (285 *linear* and 14 *area*) throughout the 6 hours' overall duration. There are 10 geographical zones, 10 geo-fences and 350 landing sites (with a fixed range of 1 km) across this airspace. The initially generated trajectories can be seen in Fig. 11a. Note that the trajectories shown represent the

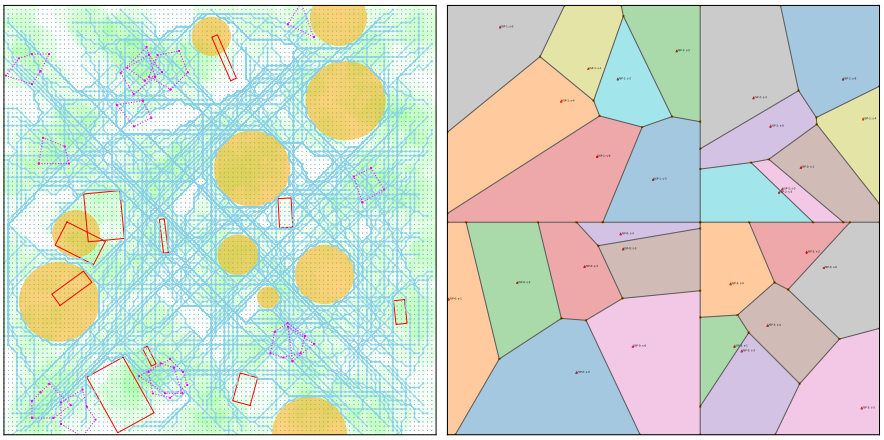

(a) Planned UAS trajectories (blue lines and purple polygons are *linear* operation and *area* operations respectively)

(b) Partitioned airspace cells (4 airspaces)

Fig. 11 Initialisation of an U-space scenario of this study.

accumulated flights generated throughout the whole duration. Meanwhile, 4 airspaces are involved, each partitioning the coverage into 7 *elementary* cells (see Fig. 11b).

Next, the trajectory and cell intersections can be derived. In average, a *linear* trajectory traverses 4.9 *elementary* cells, concerning 2 airspaces, while an *area* trajectory covers 1.6 *elementary* cells, involving 1 airspace. Then, we notice that for each *linear* trajectory, it has an average of 3.1 alternative options (a maximum of 10 is seen in a few cases), which sums up to 890 alternative trajectory options in total.

In terms of airspace structure, we set 4 as the maximum number of *elementary* cells that can be merged as one *operational* cell. Accordingly, the 28 *elementary* cells are combined into 247 different *operational* cells, each of which is associated with a particular capacity of occupancy. Furthermore, each airspace has approximately 237 selectable *configurations* (total 949 for the airspace) in each period of time.

Besides the model assumptions mentioned in Sec. II and III, additional key assumptions have been taken in the experiments:

- The DCB unit time step is 1 min and the DCB time window is considered as per 20 min (thus 18 periods within the whole duration);
- The weighted costs concerning flight priority (i.e. v_f, v_a) are randomly generated between $[1, 10]$, and the fairness factor (ϵ) is set to 0.05;
- The cost[¶] of delay (β) is 1 per minute; the cost of extra flight time due to rerouting (α) is 4 per minute; and the cost of providing a single occupancy capacity (γ) is 0.1 per 20 min;
- The occupancy capacity (per 20 min) is linearly correlated with the size of *elementary* cell, with a coefficient

[¶]The illustrative example is based on a virtual scenario and thus we do not consider a specific monetary currency unit in this study.

of 0.5 ac/km^2, but it reduces exponentially by 0.6^{n-1}, where $n \in [2, 4]$ is the number of *elementary* cells in an *operational* cell;

- The entry count capacity (per 20 min) is linearly correlated with the size of airspace's coverage, with a coefficient of 0.125 ac/km^2; and
- The speeds of *linear* operations are randomly selected between 10-50 m/s, and the durations of *area* operations are randomly set between 5-30 minutes.

B. Case studies

We consider four case studies, with or without ATO/DAC, as listed in Table 1. The DCB model presented in Sec. IV can be easily customised to realise each of these cases. Specifically, the original model represents Case-D; by disabling ATO (enforcing $z_f^{\mathcal{K}_f} = 1,\ \forall f \in \mathcal{F}$), or disabling DAC (enforcing $w_l^\tau = 1,\ \forall l \in \mathcal{L}^{(1)}, \forall \tau \in \mathbb{T}$, where $\mathcal{L}^{(1)}$ is a subset of *operational* cells that are composed of only one *elementary* cell), we can obtain Case-B and Case-C respectively; and by disabling both, we derive Case-A, where delay remains the only option. In any case, delaying the take-off time will be always available.

Table 1 Cases switching on/off ATO and DAC.

Case	Delay	ATO	DAC
Case-A	√	–	–
Case-B	√	–	√
Case-C	√	√	–
Case-D	√	√	√

Given the experience gained from our numerical experiments, we observe that the amount of delay needed in different Cases vary significantly. As a consequence, we set different values with respect to the length of $\mathcal{T}_f^j, \mathcal{T}_a^j$ that will determine the maximum allowed delay per flight, namely Case-A: 180 min, Case-B: 45 min, Case-C: 20 min, Case-D: 15 min. Note that this does not "manipulate" the results, as the actual delay is much lower than the given bound. However, this largely reduces the dimension of the optimisation model, thus can improve computational efficiency.

In this study, GAMS v.25.1 software suite has been used as the modelling tool and Gurobi v.7.5 optimiser as the solver. The experiments have been run on a 64 bit Intel® Core™ i7-8700 CPU @ 3.20GHz 6 Cores computer with 32 GB of RAM and Linux OS.

C. Demand and capacity balances

The demand and capacity consequences are presented with regards to the above Cases (post-regulation), as well as the original situation (pre-regulation). The airspace entry count capacity and the cell occupancy capacity are both assessed. Fig 12 shows the original and Case-A. In the original case, no regulation has been imposed and every single

elementary cell (i.e. 7 in each airspace) acts as the *operational* cell. The airspace's coverage, thus capacity, remains constant, so it is represented by a horizontal line in Fig. 12a. There are 124 (7*18) *operational* cells opened throughout the 18 periods of time, whose capacity also remains constant during the 18 periods, as shown in Fig. 12b. Obviously, some capacity overloads (i.e. demand higher than capacity) can be observed, which is more severe against the cell occupancy.

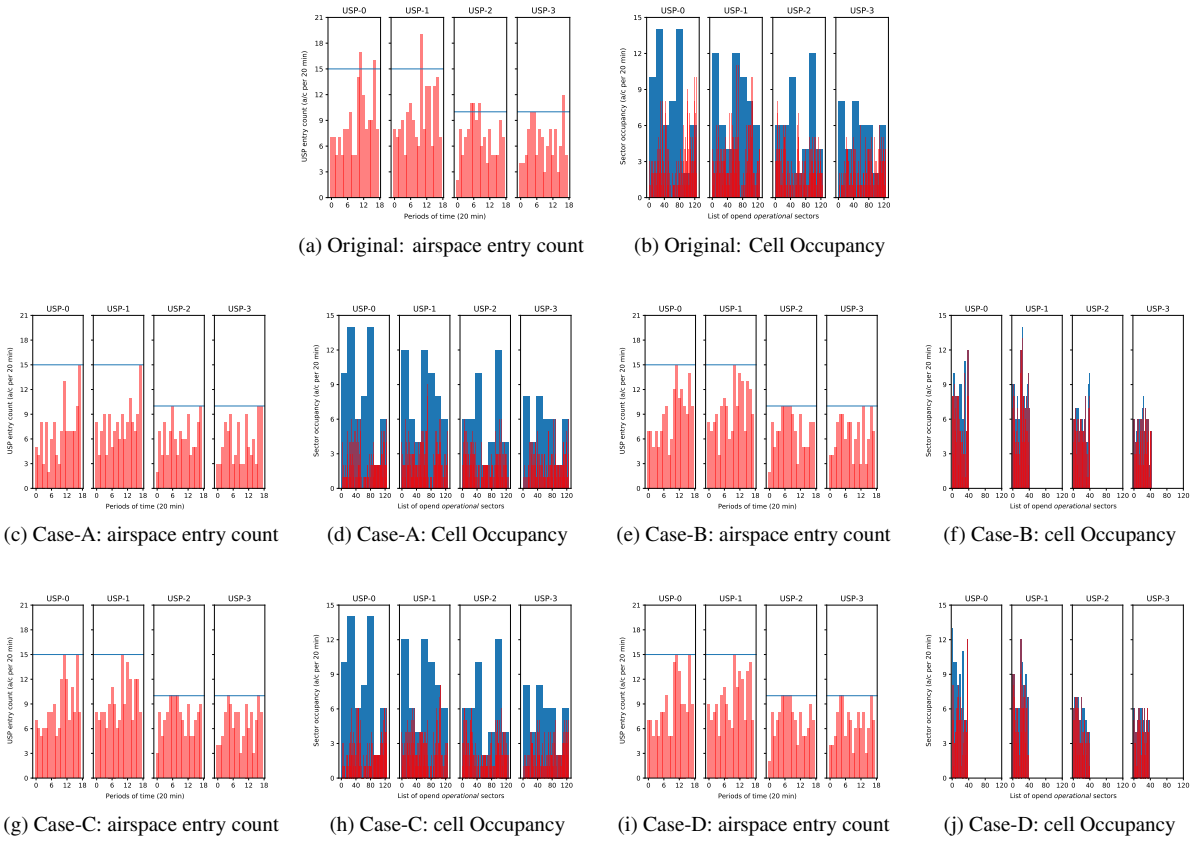

(a) Original: airspace entry count (b) Original: Cell Occupancy

(c) Case-A: airspace entry count (d) Case-A: Cell Occupancy (e) Case-B: airspace entry count (f) Case-B: cell Occupancy

(g) Case-C: airspace entry count (h) Case-C: cell Occupancy (i) Case-D: airspace entry count (j) Case-D: cell Occupancy

Fig. 12 Demand (red bars), airspace entry count capacity (blue lines) and *operational* cell occupancy capacity (blue bars).

By means of assigning delays in Case-A, all the capacity overloads can be effectively mitigated as shown in Figs. 12c and 12d. However, as the target time horizon covers only 6 hours' time, there might be a notable amount of demand to be moved out of the horizon provided their assigned delay is large. Such propagated demand will also affect the capacity in other periods, thus incurring additional delay than what is shown in this study.

Results of more advanced cases are presented in Fig. 12. In Case-B, a notable difference than the previous is that the number of opened *operational* cells is significantly less (see Fig. 12f), as some *elementary* cells are merged into one single *operational* cell. This is because, with a fixed airspace structure, the capacity provision might be not distributed properly (recall the majority unoccupied capacities in Fig. 12d). Allowing dynamic airspace configuration will however

enable the available (reduced although) capacity to be better utilised (see the minority unoccupied capacities in Fig. 12f). As such, less delay is required to meet the cell capacity, which also affects the airspace entry count, as shown in Fig. 12e). Namely, the exceeded demand will not have to be always delayed towards the end of the horizon, but instead can be distributed more evenly within the periods.

Figs. 12g and 12h present the situation in Case-C, where the airspace structure remains unchanged but we allow UAS to reroute away from the overloaded cells. This is realised by incorporating a set of alternative trajectory options submitted by each (*linear*) flight beforehand. Note that this set of trajectories involve all potential rerouting options bypassing each cell that it originally traverses. The effects are obvious, namely the demand can be redistributed not only in temporal (by means of delay), but also in spatial to less congested areas.

Based on the above discussion, we may notice that Case-B and Case-C essentially have only improved the regulation of Case-A from one thread, either demand or capacity. Finally, Case-D deals with both threads at the same time (see Fig. 12i and 12j). As such, the decisions with regards to rerouting and airspace adjustment, along with delay assignment, can be achieved in a more synchronised way. Compared with Case-B, the amount of opened *operational* cells (and thus the capacity provision) can be further reduced in Case-D. In the meantime, the required amount of delay also decreases, which will be discussed next.

D. Result comparisons

A detailed comparison in some key performance indicators (KPIs) across the Cases of the study can be seen in Table 2. The KPIs are divided into various areas, including delay, rerouting, demand, capacity, DC (demand/capacity) ratio, and solution.

We can observe that a huge amount of delay (8,098 min), being 42% flights (123) affected, is required in Case-A, if considering that the capacity overloads seem only mild (recall 12a and 12f). For Case-B and Case-C, the required delay reduces significantly to 226 min and 132 min, which suggests the effectiveness of ATO and DAC in delay reduction. The ATO seems more efficient, but it incurs some extra costs when diverting flights elsewhere, whereas DAC saves costs by means of reconfiguring the opened cells. In Case-D, their synthetic effects are revealed, with the numbers of both delay and cells further lowed down. What is more, less amount of rerouting ATO is needed (i.e., from 98 in Case-C to 76 in Case-D), meaning less extra costs for the flights.

As previously mentioned, the effects of DAC are two folded, enabling airspace structure adjustment plus flexible capacity provision. The former will affect the demand to be counted against occupancy (recall Sec. IV.F). As some *elementary* cells are merged into larger cells, part of the boundary crossings are regarded as internal movements, thus reducing the total number of occupancy (e.g. 879 in Case-B) as presented in Table 2. However, such cell merging cannot always continue, as the combined capacity declines with the number of *elementary* cells involved, and thus the accumulated demand will quickly reach the capacity. The reduction of occupancy in Case-A is simply due to the fact

Table 2 Result comparisons across the four Cases of the study.

KPI	Case-A	Case-B	Case-C	Case-D
Delay (min) - *linear*	8,053	201	124	42
Delayed flights (a/c) - *linear*	121	36	27	13
Delay (min) - *area*	45	25	8	8
Delayed flights (min) - *area*	2	3	2	2
Initial trajectory (#)	285	285	187	209
Alternative trajectory (#)	0	0	98	76
Airspace entry count - pre (a/c)	578	578	578	578
Airspace entry count - post (a/c)	479	578	578	578
Cell occupancy - pre (a/c)	1,249	1,249	1,249	1,249
Cell occupancy - post (a/c)	1,042	879	1,074	744
Airspace capacity provision (a/c)	900	900	900	900
Cell capacity provision (a/c)	3,600	1,154	3,600	1,054
Opened *operational* cells (#)	504	166	504	157
Airspace DC ratio - pre (%)	64.2	64.2	64.2	64.2
Airspace DC ratio - post (%)	53.2	64.2	64.2	64.2
Cell DC ratio - pre (%)	34.7	34.7	34.7	34.7
Cell DC ratio - post (%)	28.9	76.2	29.8	70.6
Solution gap (%)	0	1	0	0
Solution time (sec)	8	1,874	2	127

that some demand has been delayed out of the target horizon. In Case-B and Case-D, we can observe that rerouting ATO can also contribute to the occupancy reduction.

The latter effect in flexible capacity provision has been reflected in Fig. 12. A large amount of capacity that is originally planned yet not fully used can be removed or reallocated to where/when it is needed. For this reason, the provided cell capacity can be lowered down to 1,154 in Case-B and further to 1,054 in Case-D, whereas the original plan is 3,600. This can be also appreciated by the increased DC ratios (namely the cell loads) in Table 2. Without DAC, such ratios are less than 30%, but with DAC they can be improved remarkably to more than 70%.

Remember in Sec. III.A the original plan is simply to open all the *elementary* cells that are generated randomly. A more sophisticated pre-planning, given the estimated flight demand, can be done, which is exactly what Case-B does. Thus, Case-B might be regarded as airspace (capacity) planning. Based on that, the subsequent ATO can be planned more efficiently. There will be a clearer information of potential hotspots to avoid, rather than bypassing any *elementary* cell that any flight traverses.

Finally, the solution quality and speed across different Cases are also shown in Table 2. Considering the dimension and complexity of the problems, the computational performance seems acceptable (due to the model formulation), except for Case-B that is a bit under satisfactory. In light of our experimental experience, the most challenging decision part is on DAC, followed by delay assignment and ATO.

E. Further discussion

In general, the proposed approach covers a wide range of aspects in U-space, and we note that the development of specific modules is still at an initial stage. Some critical questions remain open. In terms of flight planning management, for instance, how to incorporate high-fidelity trajectory computation (e.g., 4D trajectory with wind impact) and collaborative decision making mechanisms (for fairness concerns) into the DCM service are some important questions. To tackle these issues, we expect to leverage a risk-based flight planning tool being developed in house that fully incorporates the wind effects in planning the trajectory. Also, a concept named Reasonable Time To Act (RTTA), proposed in U-space, is expected to be framed in our DCB model such that the fairness concern can be considered in a more realistic way.

With regard to airspace management, the fundamental structure may need attention, along with the capacity prediction, dynamically modification and configuration adjustment, just to name a few, on top of that airspace structure. We will follow up the latest progress of the ongoing research in these regards to update the relevant modules of this study. As for demand-capacity balancing, we may further consider what could be the potential solutions in response to non-nominal uncertainties and how to associate the solutions with flight planning and airspace management. In addition to taking conventional approaches such as stochastic programming, some promising learning-based methods can be explored as well. It may provide some added value if such methods are able to produce fast-time approximation of the optimal solution. This can be realised as a means to quickly update the solution in response to any uncertainty events.

VI. Conclusions and future work

In this paper, we demonstrated an integrated approach aimed at shaping the service of Dynamic Capacity Management (DCM) in future U-space operations. The main findings can be also applied to other ongoing UTM programmes (e.g., the Demand/Capacity Balancing service in FAA AAM, and the Flow Management service in Australia Urban ATM) to enable futuristic large-scale high-density UAS/UAM operations. The approach couples the modules of flight planning, airspace configuration and demand-capacity balancing optimisation. A simulation scenario under the proposed framework was set up to perform a group of case studies. Results proved that the integration is promising as it achieves the best outcome if comparing with other cases where module functions are partially decoupled.

We proposed the integrated DCM approach under a centralised architecture, where different inputs are collected from Operators, or their subscribed U-space Service Providers (USSPs), and modelled as a single problem. It is then assumed to be handled by a central unit who performs global optimisation such that the actors will be notified for execution of the final solution. However, implementation of the approach in such a centralised way can be problematic for scalability reasons. In future work, we will also explore the feasibility of breaking down the single (possibly large-scale) DCM problem and applying a decentralised version of the DCM service provision.

A. Additional illustrative examples

We have performed a set of additional experiments based on the same scenario discussed in Sec. V, with random samples as presented in Table 3. Comparable results of those examples are summarised in Fig. 13. The detailed outcome of the Cases can be notably impacted by different demand distribution and/or airspace configurations. However, it also proves that having ATO and DAC enabled (Case-D) would always outperform other Cases in the sense that demand and capacity can be both redistributed more flexibly to achieve their balancing.

Table 3 Parameters of randomly generated samples.

Sample	*Linear*	*Area*	Alt. trajectory	*Oper.* cell	*Configuration*
S1	299	20	723	211	749
S2	377	13	974	243	936
S3	336	13	861	237	919
S4	326	11	959	245	949
S5	319	14	855	252	1,058
S6	285	22	692	251	1,029
S7	272	13	736	252	1,018
S8	376	13	1,067	216	748
S9	309	23	710	233	875
S10	342	11	777	251	1,029

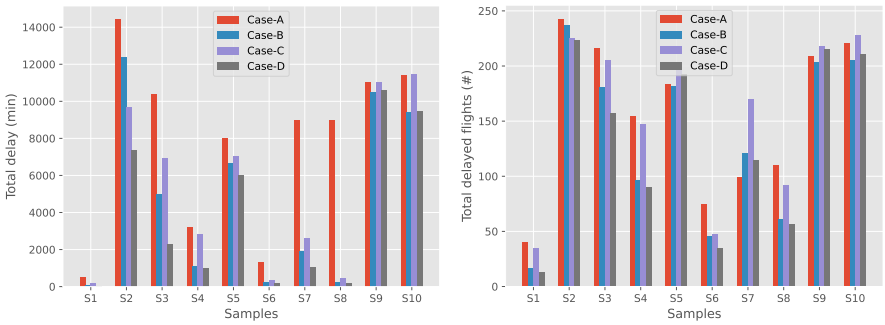

(a) Total delay

(b) Total delayed flights

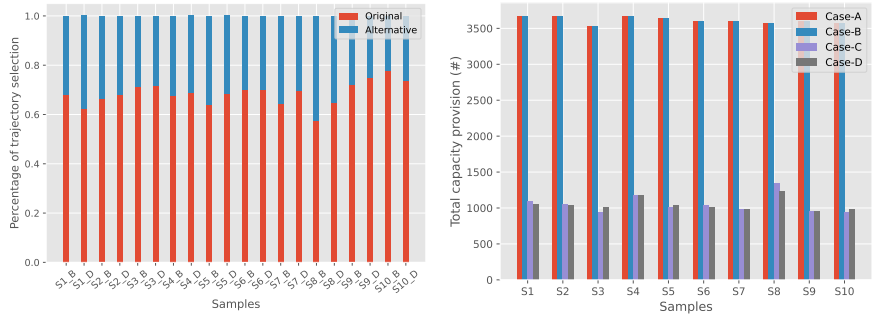

(c) Trajectory selection

(d) Total capacity provision

Fig. 13 Results of additional illustrative examples.

Abbreviation

AAM	Advanced Air Mobility
ATC	Air Traffic Control
ATCO	Air Traffic Control Officer
ATFCM	Air Traffic Flow and Capacity Management
ATM	Air Traffic Management
ATO	Alternative Trajectory Option
BVLOS	Beyond Visual Line Of Sight
DAA	Detect and Avoid
DAC	Dynamic Airspace Configuration
DCB	Demand-Capacity Balancing
DCM	Dynamic Capacity Management
SCR	Strategic Conflict Resolution
UAM	Urban Air Mobility
UAS	Unmanned Aerial Systems
UTM	UAS Traffic Management
VLL	Very Low Level
VLOS	Visual Line Of Sight

Acknowledgement

This work was partially funded by the SESAR JU under grant agreement No 101017702, as part of the European Union's Horizon 2020 research and innovation programme: AMU-LED (Air Mobility Urban - Large Experimental Demonstrations). The opinions expressed herein reflect the authors view only. Under no circumstances shall the SESAR Joint Undertaking be responsible for any use that may be made of the information contained herein.

References

[1] SESAR, "European Drones Outlook Study, unlocking the Value for Europe," Tech. rep., SESAR JU, 2016.

[2] SESAR, "European ATM Master Plan," Tech. Rep. Edition 2020, SESAR JU, 2020.

[3] SESAR, "U-space Blueprint," Tech. rep., SESAR JU, 2017.

[4] FAA, "UTM Concept of Operations Version 2.0," Tech. Rep. (UTM ConOps v2.0), Federal Aviation Administration, 2020.

[5] CAAC, "Unmanned Aircraft Traffic Management Information Service System of Civil Aviation Administration of China (UTMISS)," , 2018. URL `https://www.utmiss.com`.

[6] Airservices, "Management of Remotely Piloted Aircraft Systems (RPAS) in ATM operations: Operational Concept," Tech. Rep. (v2.0), Airservices, 2018.

[7] DECEA, "AirSpace Access Request System (SARPAS) for remotely piloted aircraft systems (RPAS) - Department of Airspace Control," , 2018. URL https://servicos.decea.gov.br/sarpas/.

[8] FAA, "Urban Air Mobility (UAM) Concept of Operations," Tech. Rep. (UAM ConOps v1.0), Federal Aviation Administration, 2020.

[9] Airservices, "Urban Traffic Management Concept of Operations," Tech. Rep. Version 1.0, Airservices Australia and Embraer Business Innovation Center, 2020.

[10] SESAR, "European ATM Master Plan: Roadmap for the safe integration of drones into all classes of airspace," Tech. rep., SESAR JU, 2018.

[11] Chin, C., Gopalakrishnan, K., Evans, A., Egorov, M., and Balakrishnan, H., "Tradeoffs between Efficiency and Fairness in Unmanned Aircraft Systems Traffic Management," *Proceedings of the 9th International Conference on Research in Air Transportation (ICRAT)*, Castelldefels, Catalonia, Spain, 2020.

[12] Bertsimas, D., and Patterson, S. S., "The air traffic flow management problem with enroute capacities," *Operations research*, Vol. 46, No. 3, 1998, pp. 406–422. doi:10.1287/opre.46.3.406.

[13] Bertsimas, D., and Gupta, S., "Fairness and collaboration in network air traffic flow management: an optimization approach," *Transportation Science*, Vol. 50, No. 1, 2015, pp. 57–76. doi:10.1287/trsc.2014.0567.

[14] Balakrishnan, H., and Chandran, B., "A Distributed Framework for Traffic Flow Management in the Presence of Unmanned Aircraft," *Proceedings of the 12th USA/Europe Air Traffic Management Research and Development Seminar (ATM2017)*, Seattle, Washington, US, 2017.

[15] Jang, D.-S., Ippolito, C. A., Sankararaman, S., and Stepanyan, V., "Concepts of airspace structures and system analysis for uas traffic flows for urban areas," *AIAA Information Systems-AIAA Infotech @ Aerospace*, Grapevine, Texas, US, 2017, p. 0449.

[16] Bayen, A. M., Raffard, R. L., and Tomlin, C. J., "Eulerian network model of air traffic flow in congested areas," *Proceedings of the 2004 American Control Conference*, Vol. 6, IEEE, Boston, MA, US, 2004, pp. 5520–5526.

[17] Menon, P. K., Sweriduk, G. D., Lam, T., Diaz, G., and Bilimoria, K. D., "Computer-aided Eulerian air traffic flow modeling and predictive control," *Journal of Guidance, Control, and Dynamics*, Vol. 29, No. 1, 2006, pp. 12–19.

[18] Xue, M., "Airspace sector redesign based on Voronoi diagrams," *Journal of Aerospace Computing, Information, and Communication*, Vol. 6, No. 12, 2009, pp. 624–634.

[19] Tang, J., Alam, S., Lokan, C., and Abbass, H. A., "A multi-objective approach for dynamic airspace sectorization using agent based and geometric models," *Transportation research part C: Emerging technologies*, Vol. 21, No. 1, 2012, pp. 89–121.

[20] FAA, "National airspace redesign strategic management plan," Tech. Rep. Revision 3b, Federal Aviation Administration, 2002.

[21] Mannino, C., Nakkerud, A., and Sartor, G., "Air traffic flow management with layered workload constraints," *Computers & operations research*, Vol. 127, 2021, p. 105159.

[22] Sachatny, D., and Henderson, T. C., "A Lane-Based Approach for Large-Scale Strategic Conflict Management for UAS Service Suppliers," *Proceedings of the 2019 International Conference on Unmanned Aircraft Systems (ICUAS)*, IEEE, Atlanta, GA, US, 2019, pp. 937–945.

[23] Doole, M., Ellerbroek, J., Knoop, V. L., and Hoekstra, J. M., "Constrained Urban Airspace Design for Large-Scale Drone-Based Delivery Traffic," *Aerospace*, Vol. 8, 2021, pp. 38–60. doi:10.3390/aerospace8020038.

[24] Hoekstra, J. M., Ellerbroek, J., Sunil, E., and Maas, J., "Geovectoring: reducing traffic complexity to increase the capacity of uav airspace," *Proceedings of the 8th International Conference on Research in Air Transportation (ICRAT)*, Castelldefels, Catalonia, Spain, 2018.

[25] Pongsakornsathien, N., Bijjahalli, S., Gardi, A., Symons, A., Xi, Y., Sabatini, R., and Kistan, T., "A Performance-Based Airspace Model for Unmanned Aircraft Systems Traffic Management," *Aerospace*, Vol. 7, No. 11, 2020, p. 154.

[26] DLR, "DLR Blueprint: Concept for Urban Airspace Integration - Integrating UAS into the future aviation system, a flexible approach enabling large-scale UAS operations," Tech. Rep. Version 1.0, Institute of Flight Guidance, 2017.

[27] AirMap, "Advance your UAS Operations with Airspace, Flight, and Capture Automation," , 2020. URL `https://www.airmap.com/operators`.

[28] DJI, "DJIFlightPlanner," , 2020. URL `https://www.djiflightplanner.com`.

[29] Chai, R., Tsourdos, A., Savvaris, A., Wang, S., Xia, Y., and Chai, S., "Fast Generation of Chance-Constrained Flight Trajectory for Unmanned Vehicles," *IEEE Transactions on Aerospace and Electronic Systems*, Vol. 57, 2021, pp. 1028–1054. doi:10.1109/TAES.2020.3037417.

[30] Hong, H., Piprek, P., Afonso, R. J. M., and Holzapfel, F., "Trigonometric Series-Based Smooth Flight Trajectory Generation," *IEEE Transactions on Aerospace and Electronic Systems*, Vol. 57, 2021, pp. 721–728. doi:10.1109/TAES.2020.3008576.

[31] Bae, S., Shin, H.-S., and Tsourdos, A., "A New Graph-Based Flight Planning Algorithm for Unmanned Aircraft System Traffic Management," *2018 IEEE/AIAA 37th Digital Avionics Systems Conference (DASC)*, 2018.

[32] Chakrabarty, A., and Ippolito, C., "Autonomous flight for Multi-copters flying in UTM-TCL4+ sharing common airspace," *AIAA Scitech 2020 Forum*, 2020.

[33] CORUS, "U-space Concept of Operations," Tech. Rep. Edition 03.00.02, SESAR JU, 2019.

[34] EUROCONTROL, "UAS ATM Integration: Operational Concept," Tech. Rep. Edition 1.0, EUROCONTROL, 2018.

[35] EASA, "Opinion No 01/2020: High-level regulatory framework for the U-space," Tech. Rep. RMT.0230, European Union Aviation Safety Agency, 2020.

[36] European Commission, "Commission Implementing Regulation (EU) 2019/947 on the rules and procedures for the operation of unmanned aircraft," Tech. Rep. 2019/947, European Union, 2019.

[37] UK CAA, "The EU UAS Regulation Package - Outline," Tech. Rep. CAP 1789, UK Civil Aviation Authority, 2020.

[38] Belobaba, P. P., Barnhart, C., and Odoni, A. R., *Airline flight operations*, John Wiley & Sons, 2009.

[39] Hart, P. E., Nilsson, N. J., and Raphael, B., "A formal basis for the heuristic determination of minimum cost paths," *IEEE transactions on Systems Science and Cybernetics*, Vol. 4, No. 2, 1968, pp. 100–107.

[40] Coulter, R. C., "Implementation of the pure pursuit path tracking algorithm," Tech. rep., Carnegie-Mellon UNIV Pittsburgh PA Robotics INST, 1992.

[41] FOCA, "Swiss U-Space ConOps Version 1.1," Tech. Rep. COO.2207.111.2.3742183, Federal Office of Civil Aviation (FOCA) and the Swiss U-Space Implementation (SUSI) Public-Private Partnership, 2020.

[42] PROSA, "Final Project Report," Tech. Rep. 00.01.04, SESAR JU, 2020.

[43] JARUS, "JARUS guidelines on Specific Operations Risk Assessment (SORA)," Tech. Rep. Edition 1.0, Joint Authorities for Rulemaking of Unmanned Systems, 2020.

[44] Aurenhammer, F., and Klein, R., "Voronoi Diagrams." *Handbook of computational geometry*, Vol. 5, No. 10, 2000, pp. 201–290.

[45] Evans, A. D., Egorov, M., and Munn, S., "Fairness in decentralized strategic deconfliction in UTM," *AIAA Scitech 2020 Forum*, 2020, p. 2203.

[46] Tang, Y., Xu, Y., and Inalhan, G., "Incorporating Optimisation in Strategic Conflict Resolution Service in U-space," *SIDs2021: 11th SESAR Innovation Days*, 2021.

[47] DACUS, "Drone DCB concept and process," Tech. Rep. Edition 01.00.00, SESAR JU, 2021.

[48] EUROCONTROL, "Hourly entry count versus occupancy count relationship definitions and indications (I)," Tech. Rep. EEC Note No. 15/07, EUROCONTROL Experimental Centre, 2007.